A ray-tracing analysis of the absorption of light by smooth and rough metal surfaces

D. Bergström[a)]
Department of Engineering, Physics and Mathematics, Mid Sweden University, S-831 25 Östersund, Sweden and Division of Manufacturing Systems Engineering, Luleå University of Technology, S-971 87 Luleå, Sweden

J. Powell[b)]
Laser Expertise Ltd., Nottingham NG7 2TR, United Kingdom and Division of Manufacturing Systems Engineering, Luleå University of Technology, S-971 87 Luleå, Sweden

A. F. H. Kaplan[c)]
Division of Manufacturing Systems Engineering, Luleå University of Technology, S-971 87 Luleå, Sweden

(Received 23 February 2007; accepted 4 April 2007; published online 1 June 2007)

Ray tracing has been employed to investigate the absorption of light by smooth and random rough metal surfaces. For normally incident light the absorptance of the surface increases with surface roughness. However, for light incident at a tangent to the surface the absorptance-surface roughness relationship is more complex. For example, in certain cases the absorptance can rise, fall, and rise again as the surface roughness increases. In this paper this complex absorptance-roughness relationship is defined and explained. The wavelengths of the light chosen for this study correspond to the primary and secondary output wavelengths of Nd:YAG lasers. © *2007 American Institute of Physics*. [DOI: 10.1063/1.2738417]

I. INTRODUCTION

An understanding of the various laser absorption mechanisms is of vital importance to the study of laser processing of metals. Laser absorption depends on a number of different parameters, involving both laser and metal properties.[1] Due to the very short penetration depths in metals for infrared and visible light (in the order of tens of nanometers), absorption is very much a surface phenomenon and depends very strongly upon the surface properties of the metal such as the roughness and texture and the existence and structure of oxide layers.

In this paper, Monte Carlo simulations are used to numerically calculate the absorptance of one-dimensional Gaussian random rough metal surfaces with various mean slopes (roughness) using the geometric optics (GO) approximation. The GO approximation is a commonly used approximation in rough surface scattering theory,[2–6] due to its relatively simple numerical implementation and the reduced computational requirements compared to the numerical integration techniques needed for rigorous electromagnetic wave analysis.[7–11] The approximation is a ray-tracing approach, where energy bundles are traced throughout their interactions with the surface until they leave it. The approximation is regarded as valid when the normalized correlation length, τ/λ, as well as the normalized rms roughness, σ/λ, are larger than unity (λ being the wavelength of the light involved). Tang *et al.*[2] have shown that the GO approximation corresponds well to the exact wave-theoretical methods for $\sigma\cos(\theta_0)/\lambda > 0.17$ (θ_0 being the angle of incidence; $\theta_0 = 0°$ meaning normal incidence) and for surfaces with $\sigma/\tau < 2.0$. Figure 1 and Table I show the regions of validity (the rms heights and the correlation lengths) for the scattering and absorptance results presented in this paper. Two wavelengths of importance to laser processing with metals were used; $\lambda = 1064$ nm corresponding to the fundamental wavelength of the Nd:YAG (yttrium aluminum garnet) laser and $\lambda = 532$ nm corresponding to second harmonic generated light for the same laser source. Four discrete angles of incidence were investigated: 0°, 30°, 60°, and 80°.

II. THEORY AND ANALYSIS

A. Radiative properties

When light is incident on a material surface the energy will either be reflected, transmitted, or absorbed. To describe

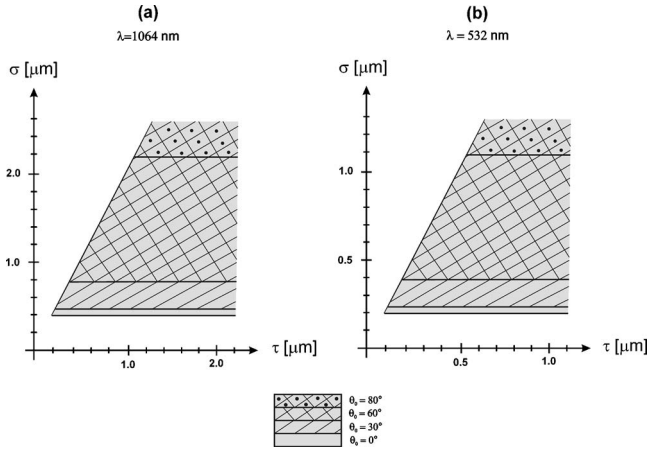

FIG. 1. Plots of the regions of validity for the geometric optics approximation for the wavelengths (a) $\lambda = 1064$ nm and (b) $\lambda = 532$ nm and the angles of incidence (0°, 30°, 60°, and 80°) used in the simulations (Ref. 2).

a)Electronic mail: david.bergstrom@miun.se
b)Electronic mail: jpowell@laserexp.co.uk
c)Electronic mail: alexander.kaplan@ltu.se

TABLE I. Region of validity of the simulation results. (Ref. 2).

θ_0 (deg)	$\lambda=532$ nm		$\lambda=1064$ nm	
	σ (μm)	τ (μm)	σ (μm)	τ (μm)
0	$\geqslant 0.20$	$\geqslant \sigma/2$	$\geqslant 0.40$	$\geqslant \sigma/2$
30	$\geqslant 0.23$	$\geqslant \sigma/2$	$\geqslant 0.47$	$\geqslant \sigma/2$
60	$\geqslant 0.40$	$\geqslant \sigma/2$	$\geqslant 0.81$	$\geqslant \sigma/2$
80	$\geqslant 1.16$	$\geqslant \sigma/2$	$\geqslant 2.23$	$\geqslant \sigma/2$

and quantify the angular distribution of the reflected or scattered light, the bidirectional reflection distribution function (BRDF) is defined as[12]

$$\rho''_\lambda(\Omega_s,\Omega_i) = \frac{\pi}{\cos(\theta_s)}\left(\frac{\frac{d\Phi_s}{d\Omega_s}}{\frac{d\Phi_i}{d\Omega_i}}\right), \tag{1}$$

where θ_s is the angle of scattered light, Φ_i and Φ_s are the incident and scattered radiant powers, and Ω_i and Ω_s are the incident and scattered solid angles, respectively. A similar definition can, of course, also be made for the bidirectional transmittance. The bidirectional reflectance is a fundamental quantity in radiative theory, from which all reflective properties can be derived and is the quantity most often derived in scattering models.

Integration of the bidirectional reflectance over the entire hemisphere yields the directional-hemispherical reflectance[12]

$$\rho'_\lambda(\Omega_i) = \frac{1}{\pi}\int_{2\pi} \rho''_\lambda(\Omega_s,\Omega_i)\cos(\theta_s)d\Omega_s. \tag{2}$$

For opaque materials such as metals (except when dealing with extremely thin films), all nonreflected light can be regarded as absorbed and by conservation of energy the spectral directional absorptance can be found from

$$A'_\lambda(\Omega_i) = 1 - \rho'_\lambda(\Omega_i). \tag{3}$$

Since there exists a direct correspondance between emittance and absorptance from Kirchhoff's law in thermodynamics, BRDF models in scattering theory can also be used to quantify the emissive properties of a material body.

B. Gaussian random rough surfaces

In light scattering theory there are two main classes of models used to describe rough surfaces: surfaces of precisely given profiles (sinusoidal, sawtooth, rectangular, etc.) and surfaces with random irregularities. These classes are named deterministic and random rough surfaces, respectively, and usually differ in their general treatment and in their applications. The treatment is a lot simpler for the first class, but most naturally occurring and man-made surfaces fall in the latter category.

A random rough surface, given by the function $z=\zeta(x,y)$, is described in statistical terms using two distribution functions, the height probability distribution, $p(\zeta(x,y))$, and the autocovariance function, $C(\tau)$. The height probability distribution describes the surface height deviation from a certain mean reference level (usually $\langle\zeta(x,y)\rangle=0$) and the autocovariance function describes the variance of these heights laterally along the surface (i.e., the crowdedness of the hills and valleys—see Fig. 2). A commonly used model is to approximate the height probability distribution as a Gaussian. Thomas[13] has demonstrated that this Gaussian assumption is valid as long as the height at any point on the surface is not produced by a single one-off event (which is true of most surfaces). The Gaussian height probability assumption gives us

$$p(\zeta) = \frac{1}{\sigma\sqrt{2\pi}}e^{-\zeta^2/2\sigma^2}, \tag{4}$$

where σ is the root mean square (rms) height (which equals the standard deviation). The autocovariance function can be defined in various ways. It is most common to use either a Gaussian or an exponential function. In this paper we assume it is described by a Gaussian so that

$$C(\tau) = \langle\zeta(x_1)\zeta(x_2)\rangle = \sigma^2\exp\left(-\frac{|x_1-x_2|^2}{\tau^2}\right), \tag{5}$$

where x_1 and x_2 are two different points along the surface and τ is the correlation length [see Fig. 2 for two surfaces with the same rms height ($\sigma=1$ μm) but with different correlation lengths]. For random rough surfaces where both the rms height distribution function and the autocovariance function are given by Gaussians (as above), it can be shown[14] that the mean slope will be given by $\sqrt{2}\sigma/\tau$. For simplicity

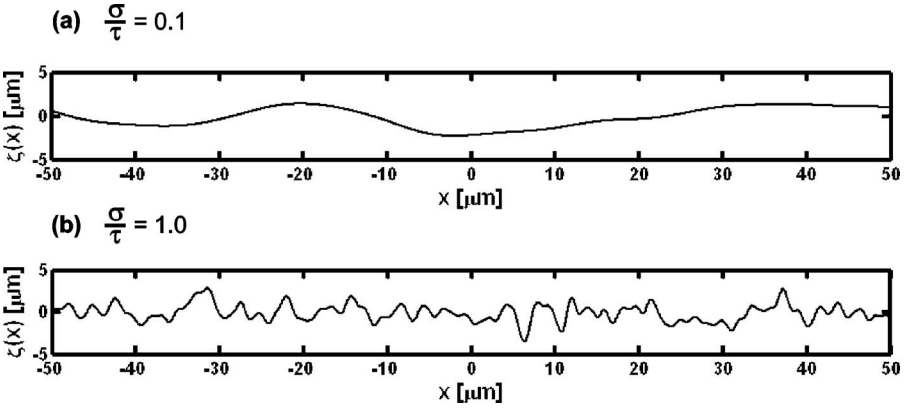

FIG. 2. Two Gaussian random rough surfaces with the same rms height ($\sigma=1$ μm) but with different correlation lengths. The profile in (a) has correlation length $\tau=10$ μm while the profile shown in (b) has $\tau=1$ μm.

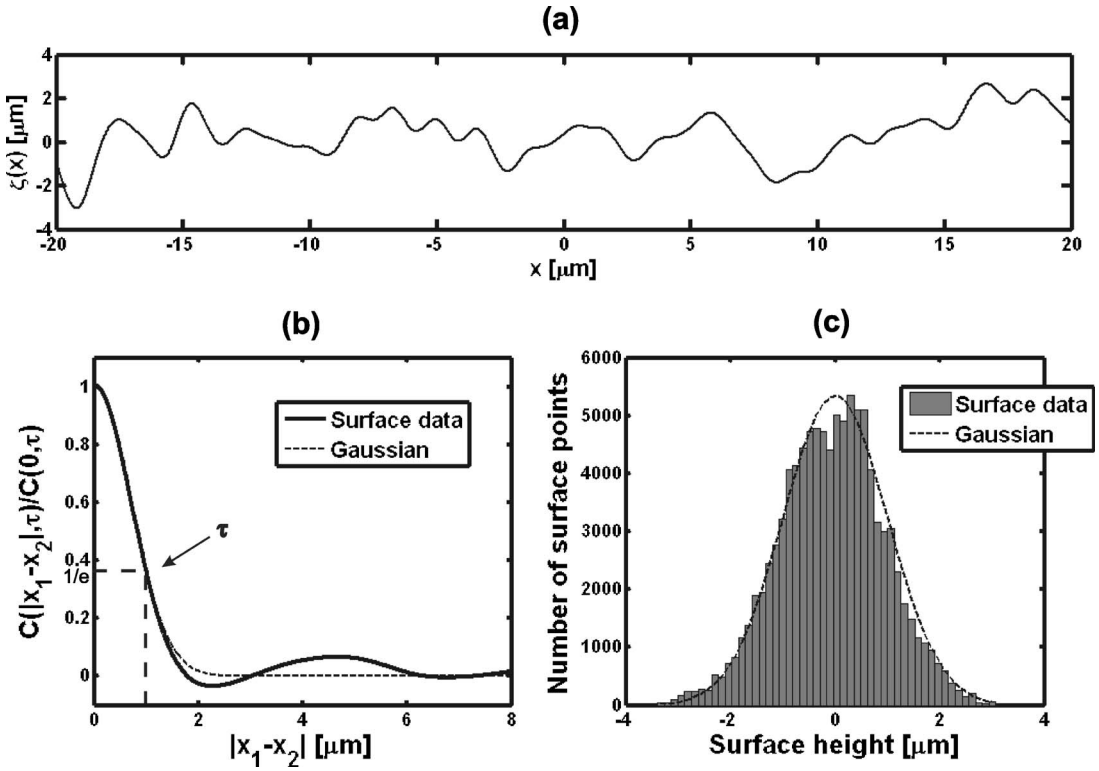

FIG. 3. (a) shows a realization of a Gaussian random rough surface using the spectrum method with $\sigma=\tau=1$ μm. (b) displays the normalized autocovariance function from the surface data compared to an exact Gaussian, while (c) plots the surface height distribution in comparison with an exact Gaussian.

the factor of $\sqrt{2}$ will be omitted in the following treatment and when we speak of the mean slope or slope we will only use the ratio σ/τ.

For simulation purposes, one-dimensional Gaussian random rough surfaces of this kind can easily be generated using the spectrum method by Thorsos.[15] The method starts with the Fourier transform of the autocovariance function in Eq. (5), which yields the power spectral density function

$$W(k_x) = \Im[C(x)](k_x) = \frac{\sigma^2\tau^2}{4\pi}\exp\left(-\frac{k_x^2\tau^2}{4}\right), \tag{6}$$

where $\Im$ denotes the Fourier transform and k_x is the variable in the spatial frequency domain.

This power spectral density function is then related to the discrete Fourier transform of the height function through the following relationship:

$$F(k_{x_m}) = 2\pi L\sqrt{W(k_{x_m})} \times \begin{cases} [N(0,1)+iN(0,1)]/\sqrt{2}, & m \neq 0, N/2 \\ N(0,1), & m = 0, N/2, \end{cases} \tag{7}$$

where $k_{x_m}=2\pi m/L$, L is the length of the rough surface, and $N(0,1)$ is a zero-mean, unit-variance normal distribution. The height function, $z=\zeta(x)$, is then obtained by taking the discrete inverse Fourier transform of $F(k_x)$,

$$z = \zeta(x) = \frac{1}{L^2}\sum_{m=-N/2}^{m=N/2-1} F(k_{x_m})\exp(ik_{x_m}x), \tag{8}$$

where for negative values of m it is necessary to use the complex conjugation of $F(k_{x_m})$ to ensure that $f(x)$ is real. Figure 3 shows one realization of a random rough surface using the method described above, together with the height distribution function and the normalized autocovariance function (also known as the correlation function) calculated from the generated data.

C. Geometric optics approximation

The geometric optics approximation is an approximation to the exact numerical integration methods available from electromagnetic wave theory. As an approximation it is, of course, limited to certain roughness parameters (as depicted in Fig. 1), but contrary to many other approximate methods, such as the Kirchhoff approximation,[15–18] the small perturbation theory,[17–19] the phase perturbation theory,[20,21] and the small slope approximation,[22,23] it is a method that naturally incorporates both shadowing and multiple scattering (see Fig. 4). It is also easily implemented for computational purposes, using intuitive geometrical arguments.

The GO approximation is a ray-tracing approach where the incident energy bundle is traced through its interactions with the surface until it leaves the surface. The surface is

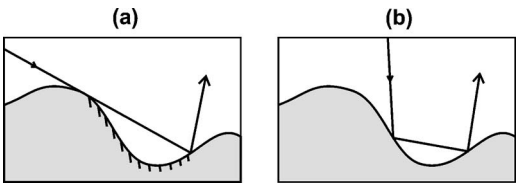

FIG. 4. (a) depicts shadowing where a part of the surface is not "seen" from the incident direction, while (b) is an illustration of multiple scattering (second order in this case).

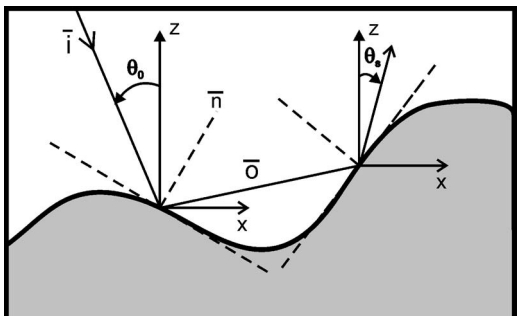

FIG. 5. Rough surface scattering geometry where $\bar{i}$ and $\bar{o}$ are the incident and scattered rays, respectively, and $\bar{n}$ is the surface normal. θ_0 and θ_s are the angles of incidence and scattering, respectively (notice their definition of positive direction).

approximated as locally smooth so that each scattering event on the surface is treated as a specular reflection (this is known as the Fresnel approximation).

The successive steps of the ray-tracing algorithm will now be explained.

Step 1. The first step consists of generating the rough surface, using, for instance, the spectrum method outlined in Sec. II B. The slopes and normals of all points are calculated and the angle of incidence of the light $(-90° < \theta_0 < 90°)$ is selected.

Step 2. A first reflection point is then chosen. The number of first reflection points can be as large as the number of surface points and can be distributed randomly or equidistant along the surface.

Step 3. For the first reflection point chosen, a strike ability test is performed to check if the reflection point can be struck by the incident ray. The tangent angle of the reflection point is compared to the angle of the incident ray (see Fig. 5 for the scattering geometry). If the ray is incident at an angle larger than the tangent angle of the reflection point, another first reflection point is chosen.

Step 4. It is then tested whether the first reflection point is shadowed due to other irregularities along the surface. This test is of most importance for larger angles of incidence (for normal incidence it is unnecessary). The angle of the incident ray is compared to the angles of the ratio of differential changes between the first reflection point and any other point on the surface (all surface points to the left if the ray is incident from the left and all points to the right if the incident ray approaches from the right). If the ray is incident at an angle larger than the angle of any ratio of differential changes, the reflection point is shadowed and another first reflection point is selected.

Step 5. If the first reflection point is strikeable and nonshadowed, the scattered ray is then calculated using the surface normal and Snell's reflection law,

$$\bar{o} = \bar{i} - 2\bar{n}(\bar{i} \cdot \bar{n}), \tag{9}$$

where $\bar{i}$ and $\bar{o}$ are the incident and scattered rays, respectively, and $\bar{n}$ is the surface normal (see Fig. 5).

The energy of the incident ray, E_i, is calculated using

$$E_i = \cos(\theta_{\text{loc}}) \frac{L}{N \cos(\alpha)}, \tag{10}$$

where $\theta_{\text{loc}} = \theta_0 + \alpha$ is the local angle of incidence (the angle between the incident ray and the surface normal), α is the tangent angle, L is the surface length, and N is the number of surface points. In this equation, the second factor represents the locally smooth segment area, while the first factor gives the area projected normal to the incident ray. In this case we are assuming that the incident energy is equally distributed along the surface. It is also possible to use other types of distributions (e.g., a Gaussian).

The energy of the scattered ray, E_s, is then found through a multiplication of E_i with the Fresnel coefficient

$$E_s = F(n, \kappa, \theta_{\text{loc}}) E_i, \tag{11}$$

where the Fresnel coefficient[11] is a function of the local angle of incidence as well as the optical constants of the material; the refractive index n and the extinction coefficient κ (it is also dependent upon polarization, but this is not investigated in this paper where a circular polarization is used throughout all interactions). The amount of energy absorbed in the scattering event is then simply the difference in energy between incident and scattered rays.

Step 6. The existence and position of any possible second reflection point are then determined by comparing the tangent of the scattered ray with the local topology (similar to the shadowing test in step 4).

Step 7. If a new reflection point is found, the scattered ray is transformed into an incident ray and the scattering process with successive reflections is continued until the energy leaves the surface. The amount of absorbed energy is then found by subtracting the incident energy [Eq. (10)] with the energy scattered off the surface.

A new first reflection point is then selected and the ray-tracing process continues until all first reflection points have been accounted for.

Step 8. When all first reflection points have been treated, the scattered energy at each scattering angle is divided by the total amount of energy incident on the surface, which is the differential reflection coefficient. The bidirectional reflection distribution function is then found by dividing the differential reflection coefficient by the cosine of the scattering angle and the size of the scattering region $d\Omega_s$ in radians (dependent on the angular resolution required), and multiplying by π [as in Eq. (1)]. In principle the absorptance then can be calculated using Eqs. (2) and (3), i.e., through an integration of the BRDF and using energy conservation, but it is more conveniently found by dividing the total amount of absorbed light (from all scattered rays) by the total amount of incident energy.

Step 9. To get statistically accurate results, the process outlined above is then repeated for several realizations of the rough surface (with the same values for σ and τ).

Step 10. Finally the results are averaged.

III. RESULTS AND DISCUSSION

A. Scattering results

Figure 6 displays some scattering plots produced by the ray-tracing algorithm for normal incidence on pure copper surfaces with a few different values for the slope ratio σ/τ at the fundamental Nd:YAG wavelength $\lambda=1064$ nm (the complex index of refraction $n+ik$ was found from the SOPRA database[24]). These plots were numerically calculated using the average simulation results for 30 surface realizations (each surface was defined by 75 000 points using 10 000 first reflection points). In the plot the differential reflection coefficient, defined as $\rho''_\lambda \cos(\theta_s)$, is displayed versus the angle of scattering θ_s, instead of the more common BRDF, ρ''_λ, as defined in Eq. (1). The reason for this is that the differential reflection coefficient is more closely related to the amount of scattered light energy for the different directions.

For small mean slopes the scattering is typically specular in nature, where for $\sigma/\tau=0.01$ the scattered light distribution resembles a delta function around $\theta_s=0°$. For $\sigma/\tau=0.1$ light is still specularly scattered but with broadening due to small changes of the local angles of incidence. As the slope increases further, e.g., at $\sigma/\tau=0.3$, a more diffuse scattering behavior is observed where light is spread across all scattering angles. For the very rough surfaces, $\sigma/\tau=1$ and 2, backscattering (also known as retroreflection) can be seen where a significant amount of light is scattered back in approximately the incident direction [see Fig. 4(b)].

Backscattering effects are even more evident when considering the scattering of light beams with non-normal incidence, as in Figs. 7 and 8, which depict the results of the geometric optics approximation for light incident on rough surfaces with angles $\theta_0=30°$ and 60°, respectively. In both figures two peaks are visible for the surfaces with higher slopes, one for the regular specular direction and one in the backscattered direction. An off-specular peak can also be seen, especially for $\theta_0=60°$, where the maximum amount of scattered light is found at an angle smaller than the expected specular direction. Both the phenomena of off-specular peaks and backscattering have been verified experimentally by independent investigators.[25–30]

B. Absorptance results

1. Normal incidence

Figures 9(a) and 9(b) show absorptance results for light normally incident on rough copper surfaces with slopes vary-

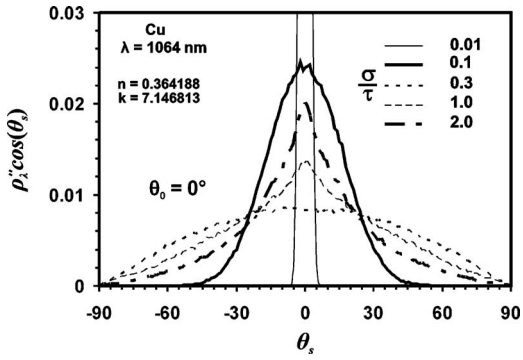

FIG. 6. Surface scattering plots for a few different mean slopes (roughness levels). The differential reflection coefficient, $\rho''_\lambda \cos(\theta_s)$, is shown vs the scattering angle θ_s for light at normal incidence.

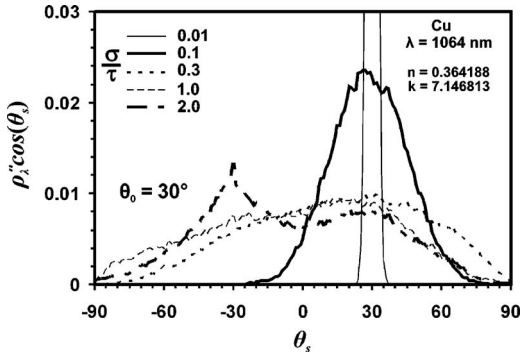

FIG. 7. Scattering plots for copper surfaces with various mean slopes (roughness levels) for light incident with an angle $\theta_0=30°$.

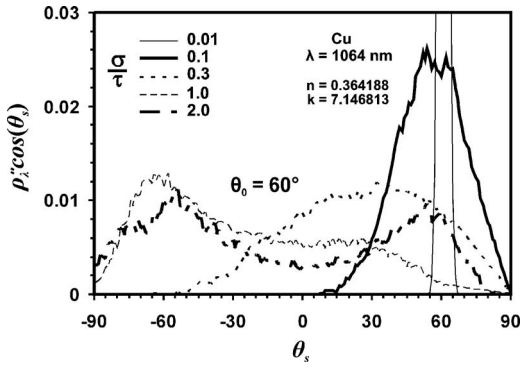

FIG. 8. Scattering plots for copper surfaces with various mean slopes (roughness levels) for light incident with an angle $\theta_0=60°$.

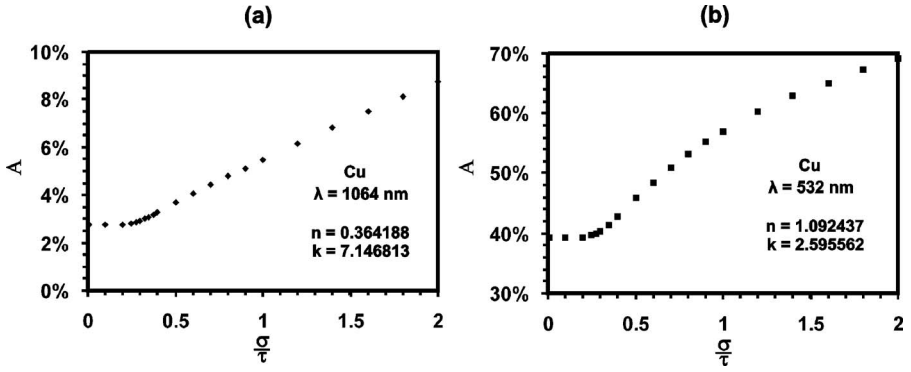

FIG. 9. Absorptance is plotted as a function of the mean slope σ/τ (roughness) for light normally incident on rough copper surfaces at (a) $\lambda=1064$ nm and (b) $\lambda=532$ nm. Optical constants taken from the SOPRA database (Ref. 24).

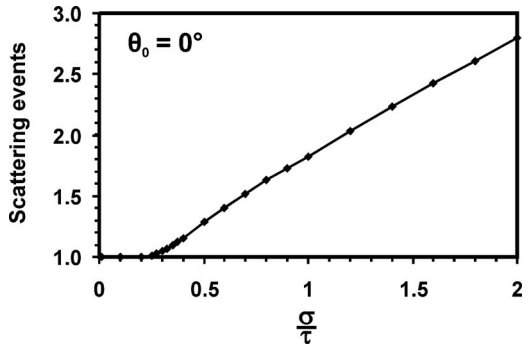

FIG. 10. The average number of scattering points per incident ray as a function of the mean slope (roughness) σ/τ for normal incidence.

ing between 0.01 and 2. The plots were generated for two sets of values for the complex refractive index representing copper at the Nd:YAG wavelengths of 1064 and 532 nm. All points in the plots are numerical results for 30 surface realizations for each slope, using 10 000 first reflection points on surfaces defined by at least 50 000 points. The standard deviation of the absorptance results presented in Fig. 9 and subsequent figures was less than 2% in all cases.

The increase in A at a mean slope of $\sigma/\tau \approx 0.2$ correlates with the threshold for multiple scattering as shown in Fig. 10, which shows the average number of scattering events as a function of the mean slope (this function is material independent as it is only dependent upon the surface topography).

This threshold is also demonstrated in Figs. 11(a) and 11(b), which are plots of the scattered energy separated into first, second, and higher order scattering for the two sets of optical constants used to generate Figs. 9(a) and 9(b). (Rays reflected only once by the surface before leaving constitute first order scattering, rays reflected twice are second order, and so on.) It can be seen, in both Figs. 11(a) and 11(b), that second order scattering starts gaining influence at about $\sigma/\tau \approx 0.2$ and third order scattering begins at $\sigma/\tau \approx 0.5$.

In Fig. 12 values of absorptance as a function of roughness are given after being normalized to the value for a flat, smooth surface (the Fresnel absorptance at normal incidence) for several metals at $\lambda = 532$ nm and $\lambda = 1064$ nm. Figure 12 demonstrates that the increase in absorptance as a function of roughness is most pronounced for high reflectivity wavelength-material combinations such as aluminum or copper at 1064 nm.

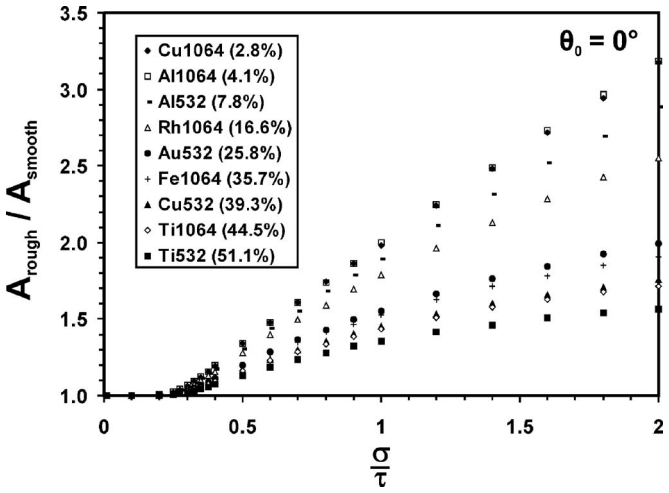

FIG. 12. Ratios of the absorptances of rough and smooth surfaces for normally incident light shown as a function of slope (roughness) for the metals listed in the legend (the number after the atomic symbol indicates the wavelength of the light involved). The smooth surface absorptance at normal incidence is given in parentheses.

Although an increase in roughness (above the threshold value of 0.2) always results in an increase in absorptance, the effect is reduced for higher absorptivity materials. This is simply a consequence of the "diminishing returns" which are to be expected when comparing multiple reflections from high and low absorptivity interactions. For example, if the absorptivity of a surface is 50% then the first scattering event will result in an absorption of 50%, and the second will result in absorption of a further 25% (of the original energy), taking the total absorption level up to 75%. If, on the other hand, the absorptivity of the material is only 10%, then the absorption figures from the primary and secondary scattering events will be 10% and 9%—making a total of 19%. This increase from 10% to 19% is considerably bigger than the increase from 50% to 75% and this is the principle demonstrated in Fig. 12.

The practical consequence of the above is that roughening the surface of a high reflectivity metal may increase its absorptance to Nd:YAG laser light by several hundred percent. The effect of roughening the surface of low reflectivity metals will not be so dramatic.

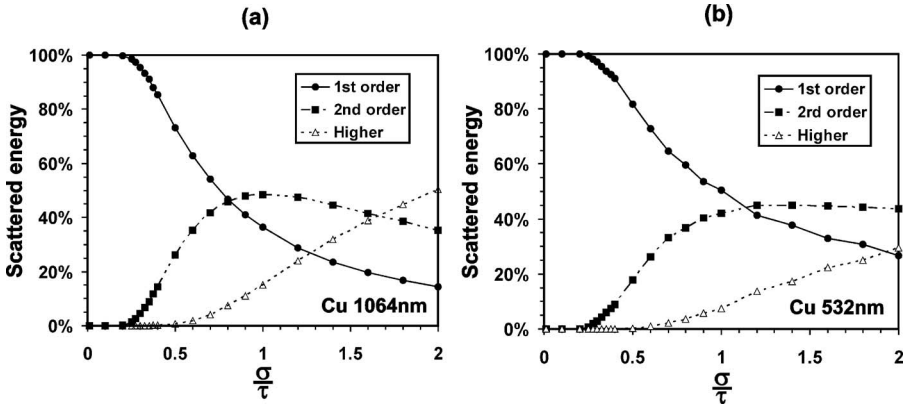

FIG. 11. Scattered energy distributed in different orders and normalized to total reflectance, for light normally incident on copper at $\lambda = 1064$ nm and at $\lambda = 532$ nm.

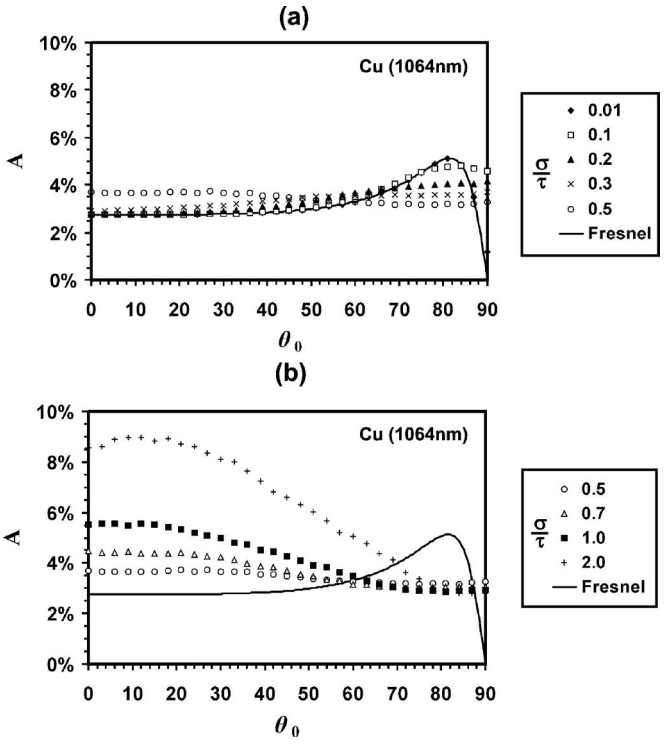

FIG. 13. The absorptance vs angle of incidence for copper at $\lambda = 1064$ nm, for a range of different slopes (roughness). In (a) $A(\theta)$ is shown for the range of small and medium slopes where $0.01 \leqslant \sigma/\tau \leqslant 0.5$, while in (b) it is given for the range of larger slopes where $0.5 \leqslant \sigma/\tau \leqslant 2.0$. The Fresnel absorptance curve has been included for reference.

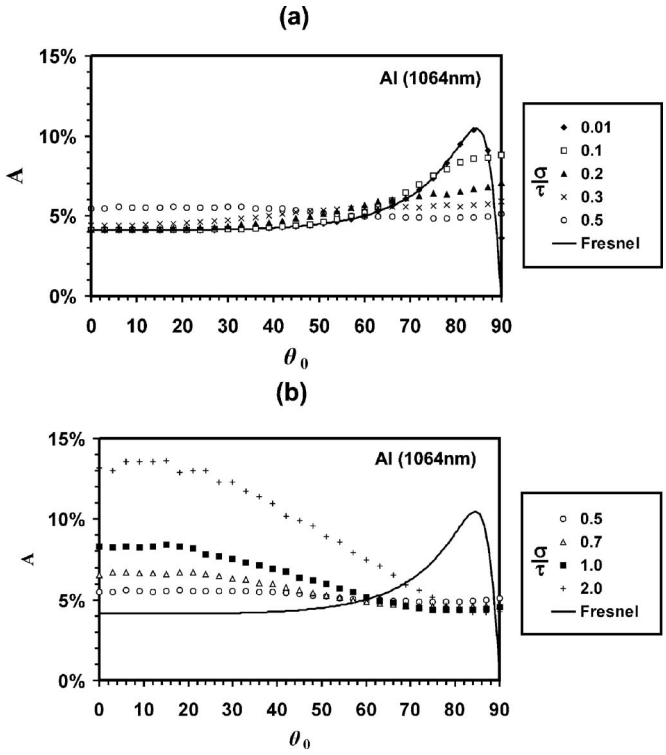

FIG. 14. The absorptance vs angle of incidence for aluminum at $\lambda = 1064$ nm, for a range of different slopes (roughness). In (a) $A(\theta)$ is shown for the range of small and medium slopes where $0.01 \leqslant \sigma/\tau \leqslant 0.5$, while in (b) it is given for the range of larger slopes where $0.5 \leqslant \sigma/\tau \leqslant 2.0$. The Fresnel absorptance curve has been included for reference.

2. Non-normal incidence and angle of incidence dependency

In some laser processing applications, such as surface treatment or laser cleaning, it is assumed that process efficiency can be increased by utilizing the Brewster maximum of the Fresnel absorptance, an angle usually situated in the range of 70°–90° (see Figs. 13 and 14 for two examples).

The Fresnel absorptance is only an approximation for perfectly smooth surfaces ($\sigma/\tau = 0$) and this dependency on angle of incidence (AOI) cannot be expected for rougher surfaces. Figures 13–15 show numerical results for the absorptance as a function of AOI for the valid slopes regime of the GO approximation. Figures 13 and 14 show results for copper and aluminum at $\lambda = 1064$ nm, respectively, while Fig. 15 shows for copper at $\lambda = 532$ nm. It can clearly be seen that the AOI dependence resembles the Fresnel curve only when $\sigma/\tau \ll 0.1$. As the slope increases up to $\sigma/\tau \approx 0.3$, the absorptance curve is flattened and both the AOI dependency and the Brewster maximum dissappear [as is seen in Figs. 13(a) and 14(a)]. As the slope is further increased a maximum close to the normal angle of incidence is established [see Figs. 13(b), 14(b), and 15(b)]. For copper at $\lambda = 532$ nm there is no pronounced Brewster maximum, as is seen in Fig. 15, but the situation is otherwise similar.

Figure 12 demonstrates that, at normal incidence, an increase in roughness has the effect of increasing the absorptance of a surface. Figures 13–15 show that this relationship does not hold true at high angles of incidence. This point is supported by a comparison of Figs. 16 and 17 which show the same data as Fig. 12 but for angles of incidence of 30°

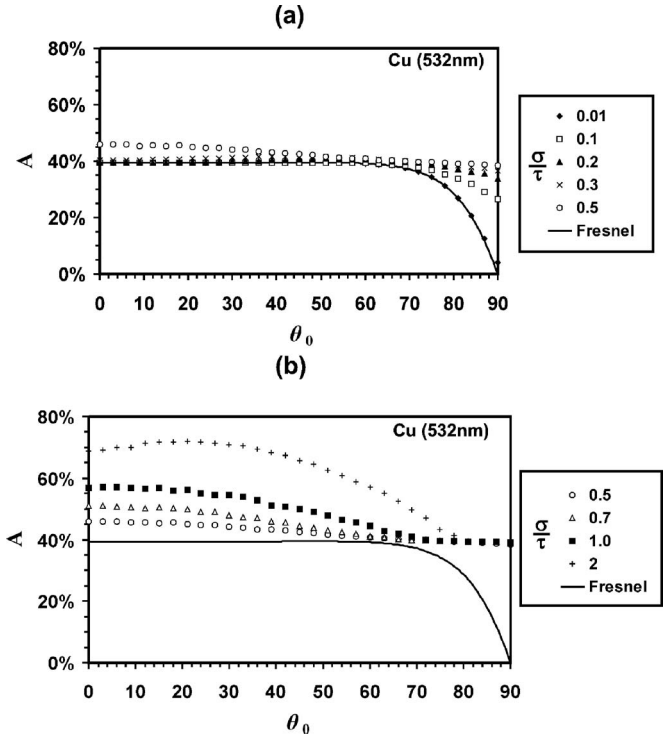

FIG. 15. The absorptance vs angle of incidence for copper at $\lambda = 532$ nm, for a range of different slopes (roughness). In (a) $A(\theta)$ is shown for the range of small and medium slopes where $0.01 \leqslant \sigma/\tau \leqslant 0.5$, while in (b) it is given for the range of larger slopes where $0.5 \leqslant \sigma/\tau \leqslant 2.0$. The Fresnel absorptance curve has been included for reference.

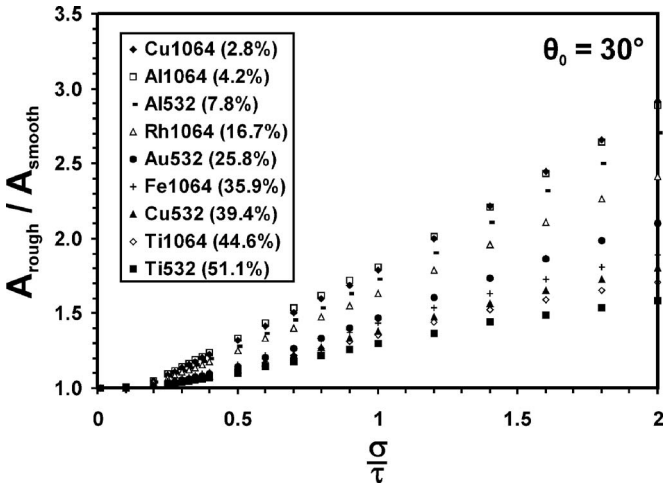

FIG. 16. Ratios of the absorptances of rough and smooth surfaces for $\theta_0=30°$ shown as a function of slope (roughness) for the metals listed in the legend (the number after the atomic symbol represents the wavelength of the light involved). The smooth surface absorptance at incidence angle $\theta_0=30°$ is given in parentheses.

and 60°, respectively. Figure 16 follows the same trends as Fig. 12 but the data presented in Fig. 17 reveal that, at high angles of incidence (60° in this case), the relationship between surface roughness and absorptance is complex. Many of the metals plotted in Fig. 17 (e.g., Al and Cu) demonstrate a decrease in absorptance with increasing roughness between the slope values of 0.2 and 0.7. Above a value of 0.7 there is a general increase in absorptance with roughness, but the lines for the different metals have differing inclinations and therefore intersect each other.

If we consider a typical set of results from Fig. 17 (e.g., Rh at 1064 nm) we can divide the surface roughness/absorptance relationship into three segments as follow.

(1) *Roughness range* $0<\sigma/\tau<0.2$. As we saw in Figs. 9–12, the absorptance of metals does not change for normally incident light in this low roughness range because only first order scattering takes place. However, the situation is different at high angles of incidence.

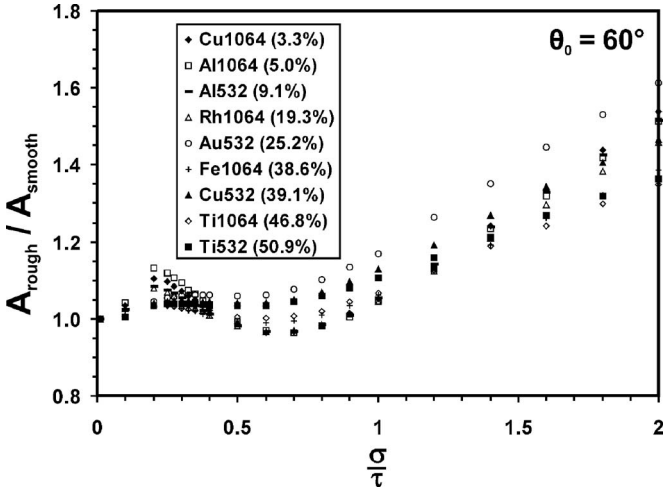

FIG. 17. Ratios of the absorptances of rough and smooth surfaces for $\theta_0=60°$ shown as a function of slope (roughness) for the metals listed in the legend (the number after the atomic symbol represents the wavelength of the light involved). The smooth surface absorptance at incidence angle $\theta_0=60°$ is given in parentheses.

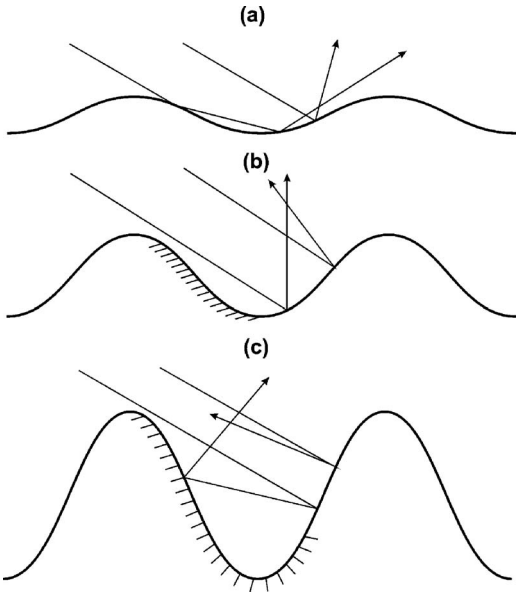

FIG. 18. Three different regions of scattering behavior for light incident with a relatively large angle, here illustrated for $\theta_0=60°$. (a) Low roughness-multiple scattering in the forward direction is possible, (b) Intermediate roughness-shadowing results in a decrease of multiple scattering in the forward direction, (c) High levels of roughness-multiple scattering in the backward direction (back scattering).

If the low roughness surface shown in Fig. 18(a) was exposed to normal incidence light there would only be a trivial amount of second order scattering. At high angles of incidence, however, second order reflections can easily take place even on low roughness surfaces—as demonstrated in Fig. 18(a). The increase of this second order scattering events with increasing roughness is the reason why the surface absorptance increases in the range $0<\sigma/\tau<0.2$.

(2) *Roughness range* $0.2<\sigma/\tau<0.6$. As the roughness of the surface is increased into this range a considerable proportion of the surface becomes shadowed as a consequence of its topology and the high angle of incidence of the light. This phenomenon is demonstrated by Fig. 18(b). To understand the effect of shadowing on the absorptance we need to refer back to Fig. 18(a); here we can see that second order reflection at a high angle of incidence must involve the reflection of the ray of both sides of the same "valley." If the roughness is low there will be no shadowing and the whole of both sides of any valley are available to take part in multiple absorption events (although not all primary reflections will give rise to secondary ones). As the roughness is increased shadowing becomes a feature and the sides of the valleys closest to the light source become increasingly unavailable as sites for primary reflections. The number of multiple absorption events will therefore decrease and this will lead to a reduction in absorptance.

(3) *Roughness range* $0.6<\sigma/\tau<2$. The increase in absorptance as the roughness increases through the range $0.6<\sigma/\tau<2$ is due to an increase in the level of backscattered multiple absorption events demonstrated by Fig.

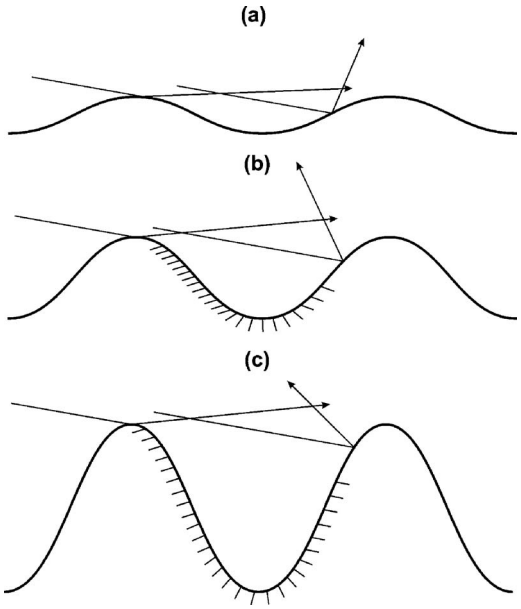

FIG. 19. Three different regions of scattering behavior for light incident at a glancing angle, here illustrated for $\theta_0=80°$. (a) Low roughness—minimal multiple scattering; (b) intermediate roughness-shadowing—minimal multiple scattering; (c) high levels of roughness—only the top part of the far valley is nonshadowed—minimal multiple scattering or backscattering.

18(c). In this case the multiple reflections once more involve both sides of the same valley but the order of reflection is reversed from the forward scattering shown in Fig. 18(c). This effect increases with surface roughness (within the limits shown here) and a gradual increase in absorptance is the result.

If the light is incident on the surface at a glancing angle the backscattering phenomenon illustrated in Fig. 18(c) becomes suppressed. Figure 19 demonstrates this point, showing the scattering experienced by a beam with $\theta_0=80°$.

Here we can see that the geometry of the situation generally favors only single scattering interactions even if the surface roughness is increased (which is confirmed by simulations, see Fig. 20). At this high angle of incidence one side of each valley is in shadow in nearly all cases. Also, the light can generally only interact with the upper part of the far slope of the valley in question. The geometry of this arrangement ensures that light is not scattered back onto the shadowed slope. Figure 21 presents the ratio of the absorptance for increasingly rough surfaces compared to the flat surface absorptance at an angle of incidence of 80°. Here we can see that the absorptance tends to level out as σ/τ rises above a value of 0.6. This is because the number of multiple scattering events does not rise with roughness (as seen in Fig. 20).

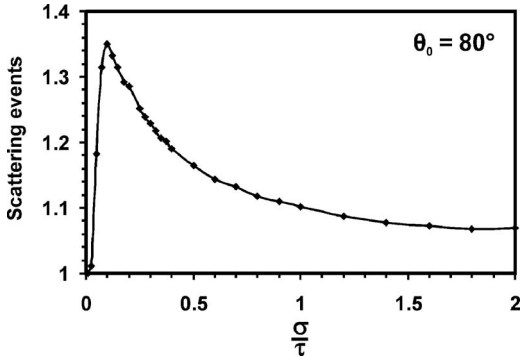

FIG. 20. The average number of scattering points per incident ray as a function of the mean slope (roughness) σ/τ for 80° incidence.

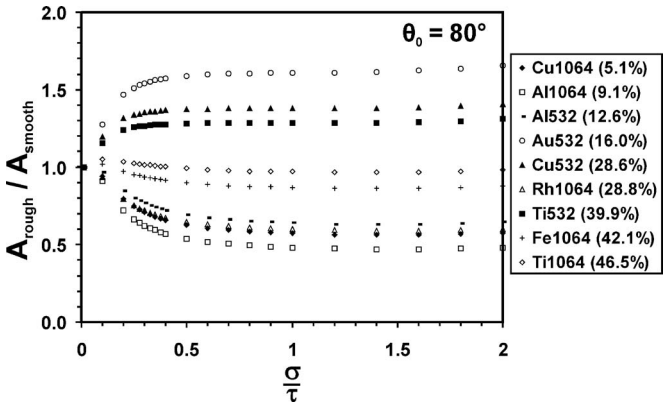

FIG. 21. Absorptance ratios shown as a function of slope (roughness) for optical constants representing the metals listed in the legend (the number after the atomic symbol represents the wavelength involved). The smooth surface absorptance at incidence angle $\theta_0=80°$ is given in parentheses.

It may seem surprising that some of the metal/wavelength combinations in Fig. 21 show a decrease in absorptance with increasing roughness and then remain at a level which is lower than 1.0 (the flat surface value). This phenomenon can be explained with the help of Fig. 22 which considers the local angle of incidence experienced by individual rays rather than the macroscopic overall angle of 80°.

Figure 22 shows that as the roughness (σ/τ or slope) increases, the average local angle of incidence changes from 80° to approximately 30° (the standard deviation curve demonstrates that, for a flat surface, the incident angle is exactly 80°, but variance around the mean increases as the roughness increases). This change in mean local angle of incidence is clearly demonstrated in Fig. 19 which shows that, as the surface roughness increases, the light interacts with an increasingly specific portion of the surface, i.e., the upper part of the far side of each valley. The geometry of this area means that the local angle of incidence is generally considerably smaller than 80°. To understand why this downwards drift in local angle of incidence gives us "A rough/A smooth" ratios of less than 1.0 (see Fig. 21) we need to refer to the absorptance versus angle of incidence curves for the materials in question.

Figure 23(a) clearly shows that, for Al at a wavelength of 532 nm, the absorptance is much greater at an angle of incidence of 80° than it is for angles of approximately 30°. This being the case it is easy to understand that, if single scattering is predominant and if an increase in surface roughness gives a decrease in local angles of incidence, the overall absorptance of the surface will decrease (which is confirmed in Fig. 21). Conversely, if we look at the absorptance versus angle of incidence curve for Au at a wavelength of 532 nm [Fig. 23(b)], we can see that a reduction in angle of incidence from 80° to 30° will result in an increase in absorptance.

This result is also confirmed in Fig. 21 which shows that, for gold, rough surfaces (with lower local angles of incidence) are more absorptive than a smooth surface.

IV. CONCLUSIONS

The conclusions below have, of course, only been demonstrated within the confines of the roughness and wavelength limits of this paper. However, the authors feel that the principles will remain valid over a much wider range of roughnesses and wavelengths. Some of the points raised in the following conclusions are well established but have been included here in the interests of providing a full set of observations.

(1) When light is normally incident on a flat smooth metal surface it is reflected in a specular manner back in the direction it came from. If the surface is slightly roughened the reflected light diverges from the specular reflection angle. If the surface is roughened beyond a certain limit then multiple reflection events take place which tend to concentrate the beam back in the direction it came from.
(2) When light is incident at an angle on a flat, smooth metal surface it is reflected off the surface at the same angle in a specular manner. If the surface is slightly roughened the beam diverges away from this specular reflection angle. If the surface is roughened above a threshold value multiple scattering can take place which, eventually, can direct a substantial proportion of the beam back in the approximate direction it came from.
(3) For normally incident light the absorptance of the surface increases with roughness after a certain roughness threshold has been exceeded. This phenomenon is the result of the onset of multiple scattering events. (Double scattering has its own roughness, threshold and triple scattering has a higher one, etc.).
(4) The increase of absorptance with roughness noted above is most pronounced for metals which have a low absorptivity in the flat, smooth state.
(5) For small angles of incidence (up to approximately 30° * in the case of this study) the change in absorptance with surface roughness follows the same trends as for normal incidence (noted above). * 0° = Normal incidence.
(6) For large angles of incidence (approximately 60° in the case of these results) absorptance first rises, then falls, then rises again as the surface roughness is increased. The initial rise is due to increasing levels of multiple scattering (the multiple scattering roughness threshold is minimized at large angles of incidence). The fall is caused by part of the surface falling into shadow, a phenomenon which inhibits multiple scattering. The eventual rise in absorptance is due to advent and rise of backscattered multiple scattering events.
(7) For very large angles of incidence (approximately 80° in the case of this work) the absorptance eventually remains fairly uniform with increasing surface roughness after rising or falling to a level above or below the reflectivity level for a smooth flat surface. The rise or fall in this case is due to the fact that the average local angle of incidence must be considered when ray tracing on rough surfaces. The average local angle of incidence falls with increasing roughness and the absorptance versus angle of incidence relationship (the Fresnel curves) for the material will determine whether the absorptance rises or falls with increasing roughness.
(8) At very large angles of incidence the light-material interaction is predominantly governed by single scattering

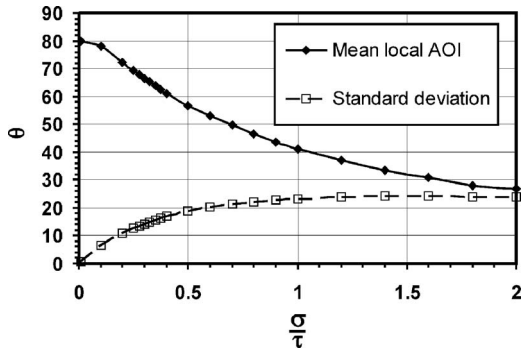

FIG. 22. Mean average local angle of incidence as a function of surface roughness (slope), for light with a global incidence of 80°.

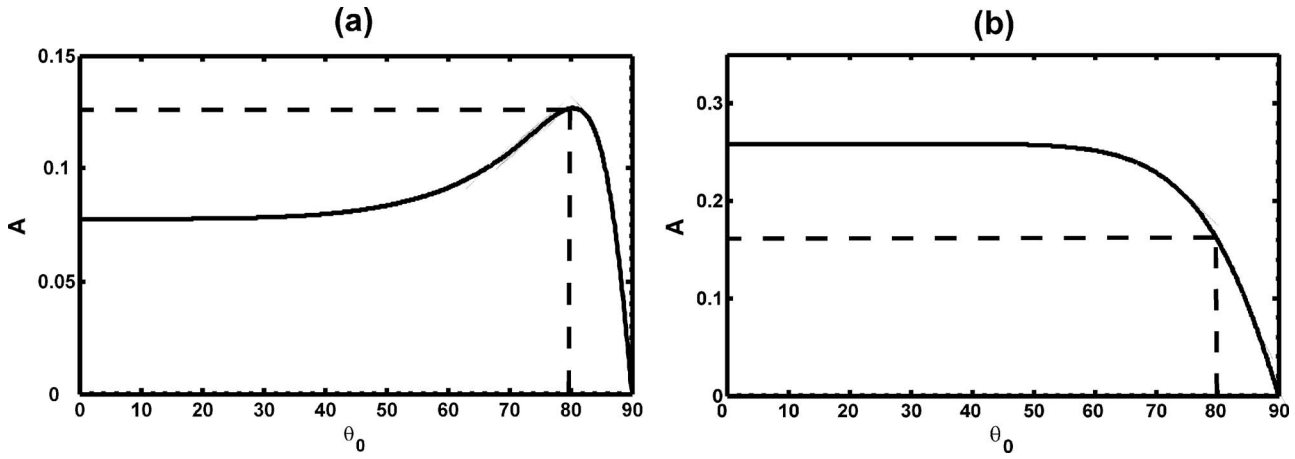

FIG. 23. Absorptance (A) vs angle of incidence (θ_0) for perfectly smooth (a) aluminum and (b) gold, both at $\lambda = 532$ nm. $A(80°)$ is indicated in the figure.

events whatever the roughness involved. This results in only small changes in absorptance with increasing roughness once the "local angle of incidence" (7 above) settles down to a fairly constant value.

[1] D. Bergström, Laser absorptance of metallic alloys to Nd:YAG and Nd:YLF laser light, Licentiate Thesis, Luleå University of Technology, 2005.
[2] K. Tang, R. Dimenna, and R. Buckius, Int. J. Heat Mass Transfer **40**, 49 (1997).
[3] K. Tang and R. Buckius, Int. J. Heat Mass Transfer **41**, 2037 (1998).
[4] K. Tang, P. Kawka, and R. Buckius, J. Thermophys. Heat Transfer **13**, 169 (1999).
[5] P. Schott, N. de Beaucoudrey, and C. Bourlier, in Proceedings of the 23rd IEEE International Geoscience and Remote Sensing Symposium, Tolhouse, France, July 21-25, 2003, p. 4214
[6] Q. Zhu, Ph.D. thesis, Georgia Institute of Technology, 2004.
[7] V. Celli, A. Maradudin, A. Marvin, and A. McGurn, J. Opt. Soc. Am. A **2**, 2225 (1985).
[8] A. Maradudin, T. Michel, A. McGurn, and E. Mendez, Ann. Phys. (N.Y.) **203**, 255 (1990).
[9] J. Gil and M. Vesperinas, J. Opt. Soc. Am. A **8**, 1270 (1991).
[10] P. Tran and A. Maradudin, Opt. Commun. **110**, 269 (1994).
[11] K. Pak, L. Tsang, H. Chan, and J. Johnson, J. Opt. Soc. Am. A **12**, 2491 (1995).
[12] M. Modest, *Radiative Heat Transfer* (Academic, San Diego, CA, 2003).
[13] T. Thomas, *Rough Surfaces* (Longman, New York, 1982).
[14] L. Tsang, J. A. Kong, and K.-H. Ding, *Scattering of Electromagnetic Waves: Theories and Applications* (Wiley Interscience, New York, 2000).
[15] E. Thorsos, J. Acoust. Soc. Am. **83**, 78 (1988).
[16] P. Beckmann and A. Spizzichino, *The Scattering of Electromagnetic Waves from Rough Surfaces* (Pergamon, New York, 1963).
[17] M. Chen and A. Fung, Radio Sci. **23**, 163 (1988).
[18] A. Navarrete, E. Chaikina, and E. Mendez, J. Opt. Technol. **69**, 71 (2002).
[19] J. Soto-Crespo and M. Nieto-Vesperinas, J. Opt. Soc. Am. A **7**, 1185 (1990).
[20] J. Shen and A. Maradudin, Phys. Rev. B **22**, 4234 (1980).
[21] S. Broshat, E. Thorsos, and A. Ishimaru, J. Electromagn. Waves Appl. **3**, 237 (1989).
[22] A. Voronovich, Waves Random Complex Media **4**, 337 (1994).
[23] A. Voronovich, *Wave Scattering from Rough Surfaces* (Springer, Berlin, 1999).
[24] SOPRA database of optical indices; http://www.sopra-sa.com/more/database.asp
[25] K. Torrance and E. Sparrow, J. Opt. Soc. Am. **57**, 1105 (1967).
[26] A. Smith, P. Muller, W. Frost, and H. Hsia, in Proceedings of the 5th AIAA Thermophysics Conference, Los Angeles, June 29–July 1, 1970, p. 249.
[27] Z. Gu, R. Dummer, A. Maradudin, and A. McGurn, Appl. Opt. **28**, 537 (1989).
[28] P. Phu, A. Ishimaru, and Y. Kuga, Radio Sci. **28**, 533 (1993).
[29] C. West and K. O'Donnell, J. Opt. Soc. Am. A **12**, 390 (1995).
[30] G. Macelloni, G. Nesti, P. Pampaloni, S. Sigismondi, D. Tarch, and S. Lolli, IEEE Trans. Geosci. Remote Sens. **GE–38**, 459 (2000).